Supporting information

for Cook *et al.* “Full-section otolith microtexture imaged by local-probe X-ray diffraction ”

Table S1

Unit cell parameters of aragonite, calcite, and vaterite. Data from Caspi *et al.* (2005), Swanson & Fuyat (1953), Hayakawa *et al.* (2008), Kamhi (1963), and Sass *et al.* (1957).

	Aragonite	Calcite	Vaterite
Ca coordination	9	6	8
System	Orthorhombic	Rhombohedral	Rhombohedral
Space group	*Pmcn*	$R\bar{3}c$	$P6_3/mmc$
a (Å)	4.96183 (1)	4.989	4.130
b (Å)	7.96914 (2)	4.989	4.130
c (Å)	5.74285 (2)	17.062	8.490
α (°)	90	90	90
β (°)	90	90	90
γ (°)	90	120	120
Unit cell volume (Å^3)	227.081	424.67	125.41

References

Caspi, E., Pokroy, B., Lee, P., Quintana, J. & Zolotoyabko, E. (2005). *Acta Crystallographica Section B-Structural Science*, **61**(Part 2), 129–132.

Hayakawa, S., Hajima, Y., Qiao, S., Namatame, H. & Hirokawa, T. (2008). *Analytical Sciences*, **24**(7), 835–837.

Kamhi, S. R. (1963). *Acta Crystallographica*, **16**(8), 770–772.

Sass, R. L., Vidale, R. & Donohue, J. (1957). *Acta Crystallographica*, **10**(9), 567–570.

Swanson, H. & Fuyat, R. (1953). *Circular of the Bureau of Standards: Standard X-ray diffraction powder patterns*. National Bureau of Standards.

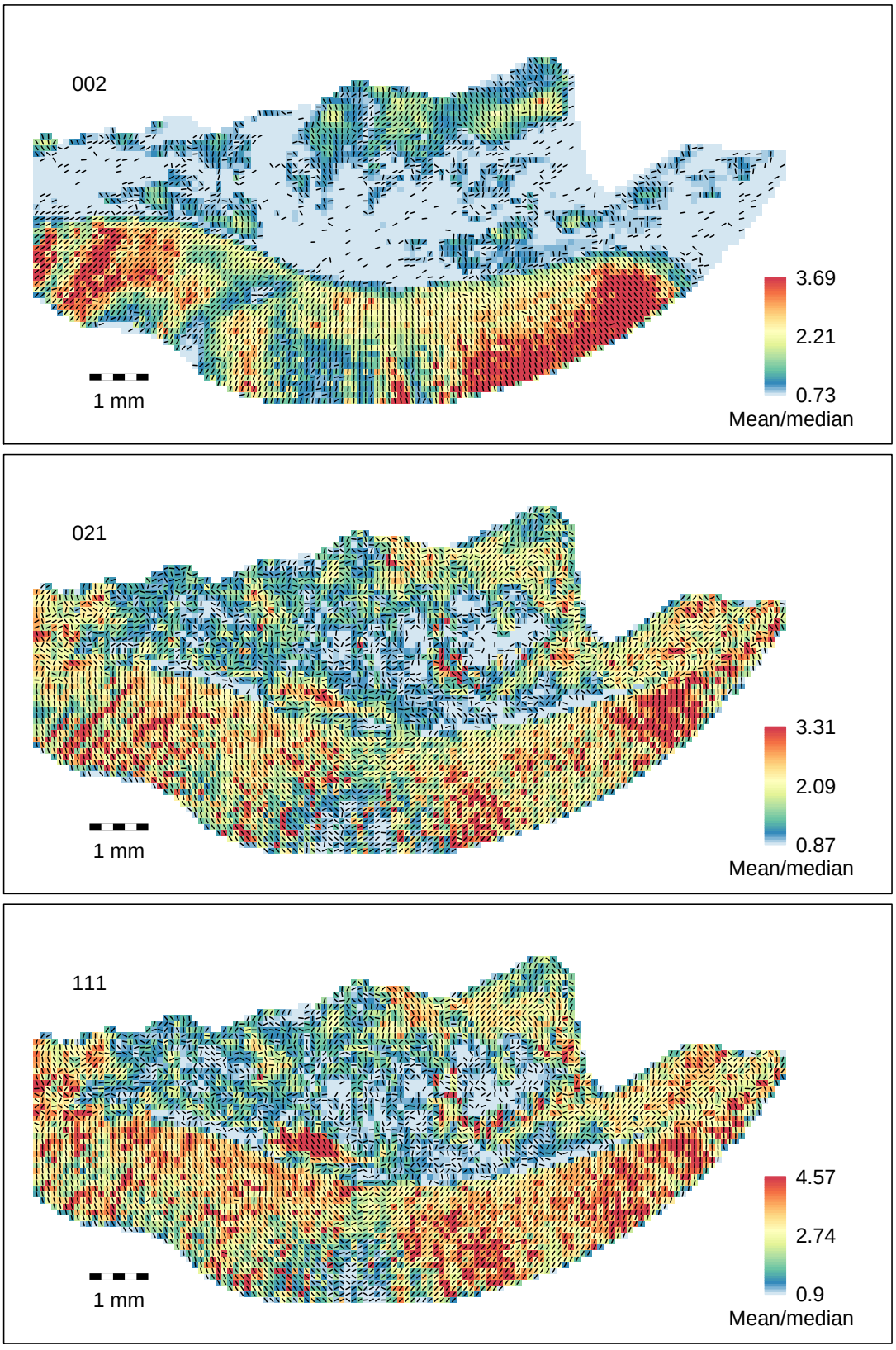

Figure S1
Orientations of 002, 021, and 111 reflections of sample 424 determined from step scan mode.

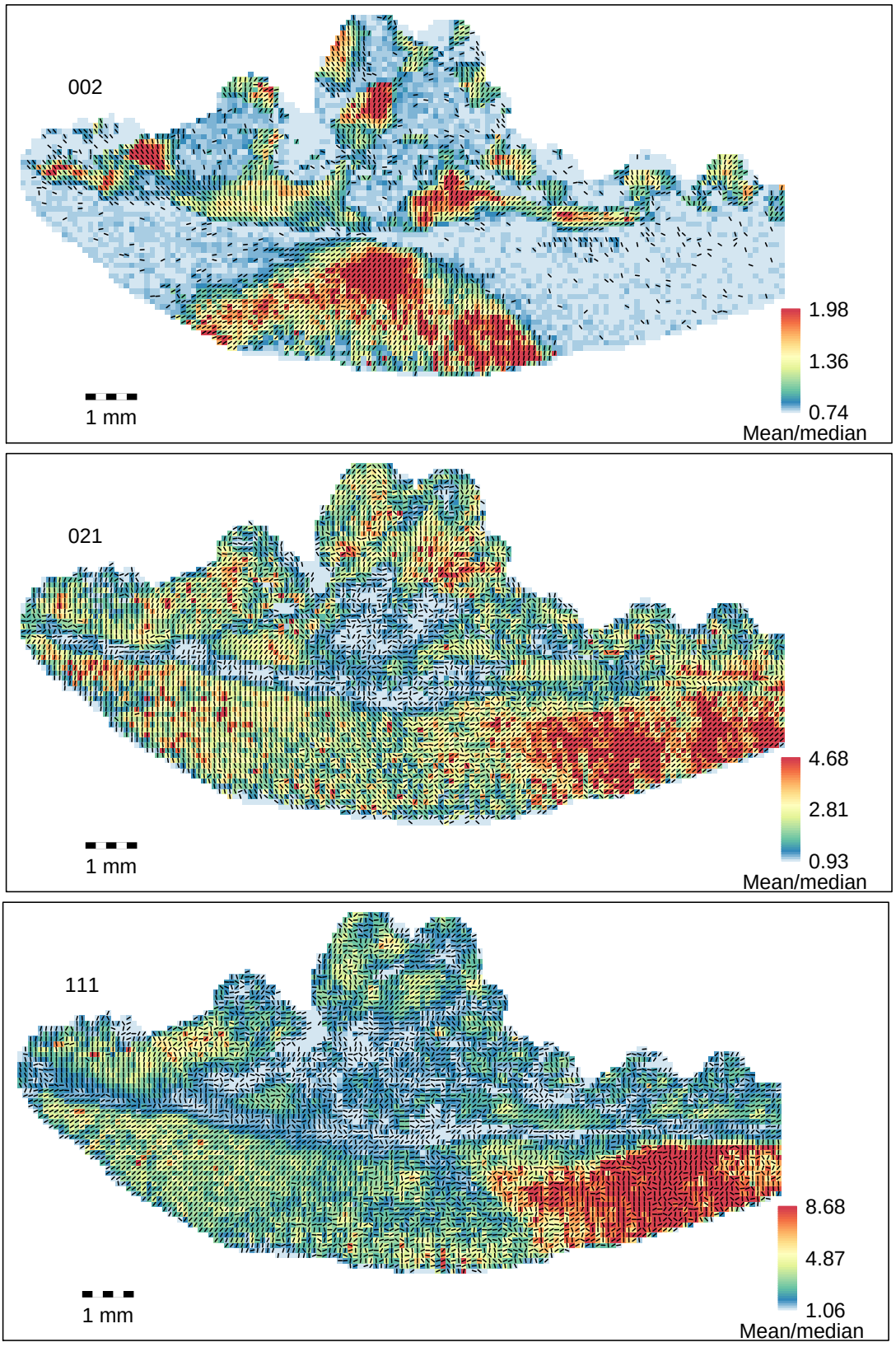

Figure S2
Orientations of 002, 021, and 111 reflections of sample QCD determined from step scan mode.

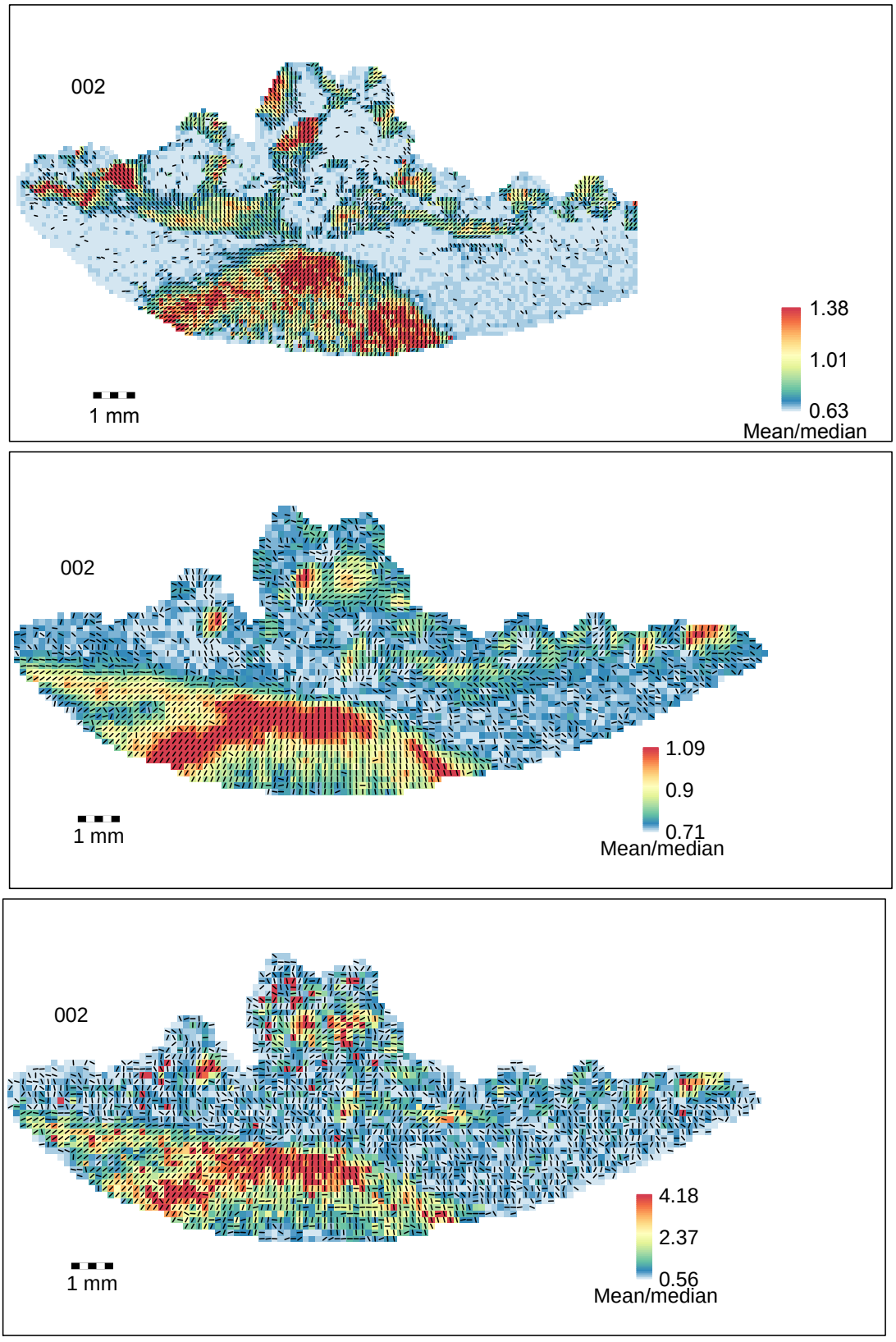

Figure S3
Orientations of 002 reflection of sample QCD, determined from step scan mode (top) and Flyscan with a 50 ms exposure (middle) and 5 ms exposure (bottom). Data quality is indicated by the ratio of mean to 75th percentile. The step scan and Flyscan measurements were carried out during separate experimental sessions with different detectors. As such, the sample mounting and accessible ψ range was different. The accessible ψ range was *ca.* 40° wider in the Flyscan measurements (Tab. 1), which permitted the observation of a continued orientation sweep toward ψ positions closer to horizontal and reveals additional information visible in the lower left corner of the sample.

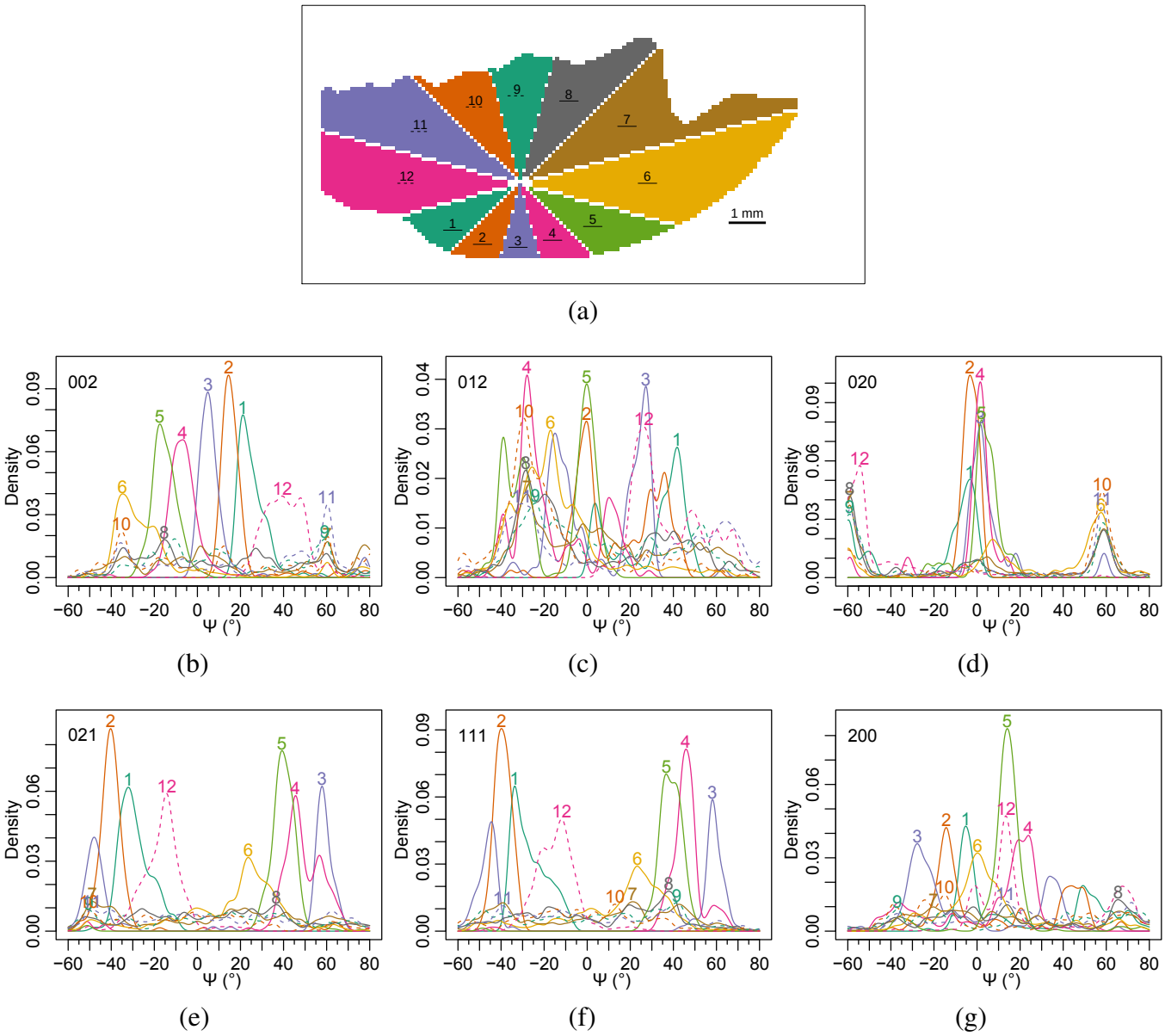

Figure S4
Correlation of crystal orientation with position on otolith 424. The otolith was divided into wedges around its core (a). For selected reflections (b-g, reflection labelled in upper left of plots) the kernel density of the ψ_0 orientations was plotted in the corresponding colour and line type (solid or dashed) to the wedges in a.

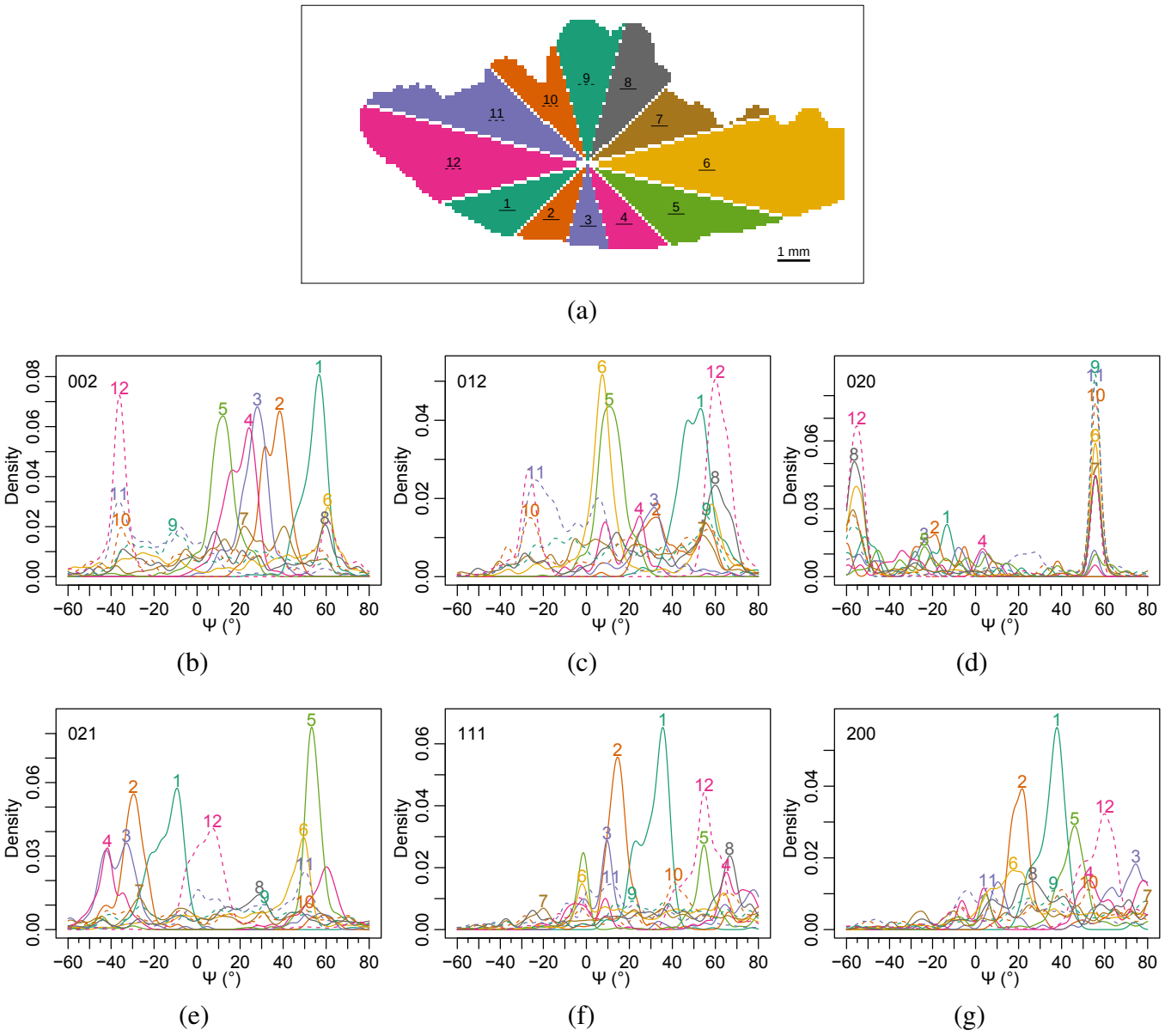

Figure S5
Correlation of crystal orientation with position on otolith QCD. The otolith was divided into wedges around its core (a). For selected reflections (b-g, reflection labelled in upper left of plots) the kernel density of the ψ_0 orientations was plotted in the corresponding colour and line type (solid or dashed) to the wedges in a.

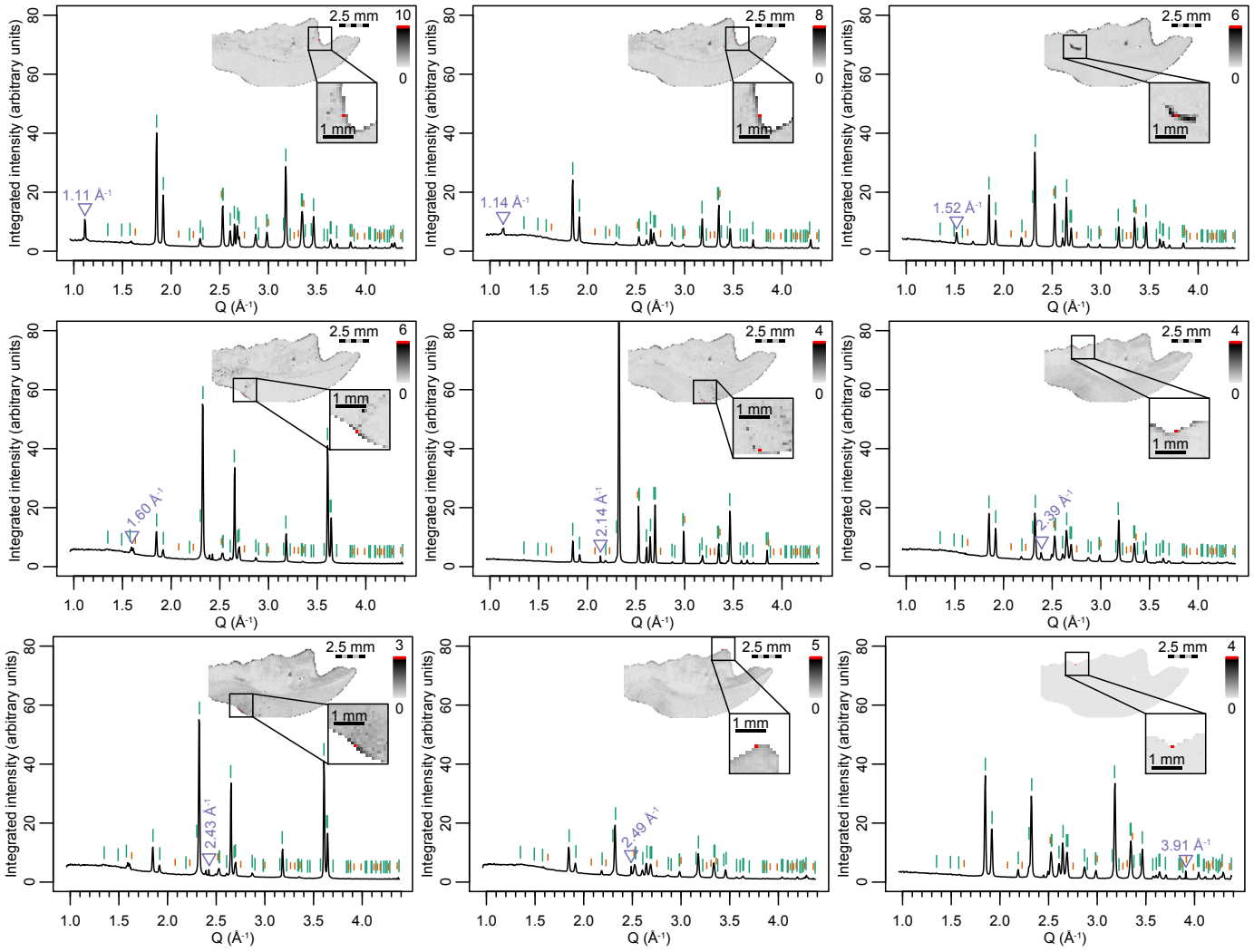

Figure S6
Identification and localisation of non-aragonite pixels in sample 424.

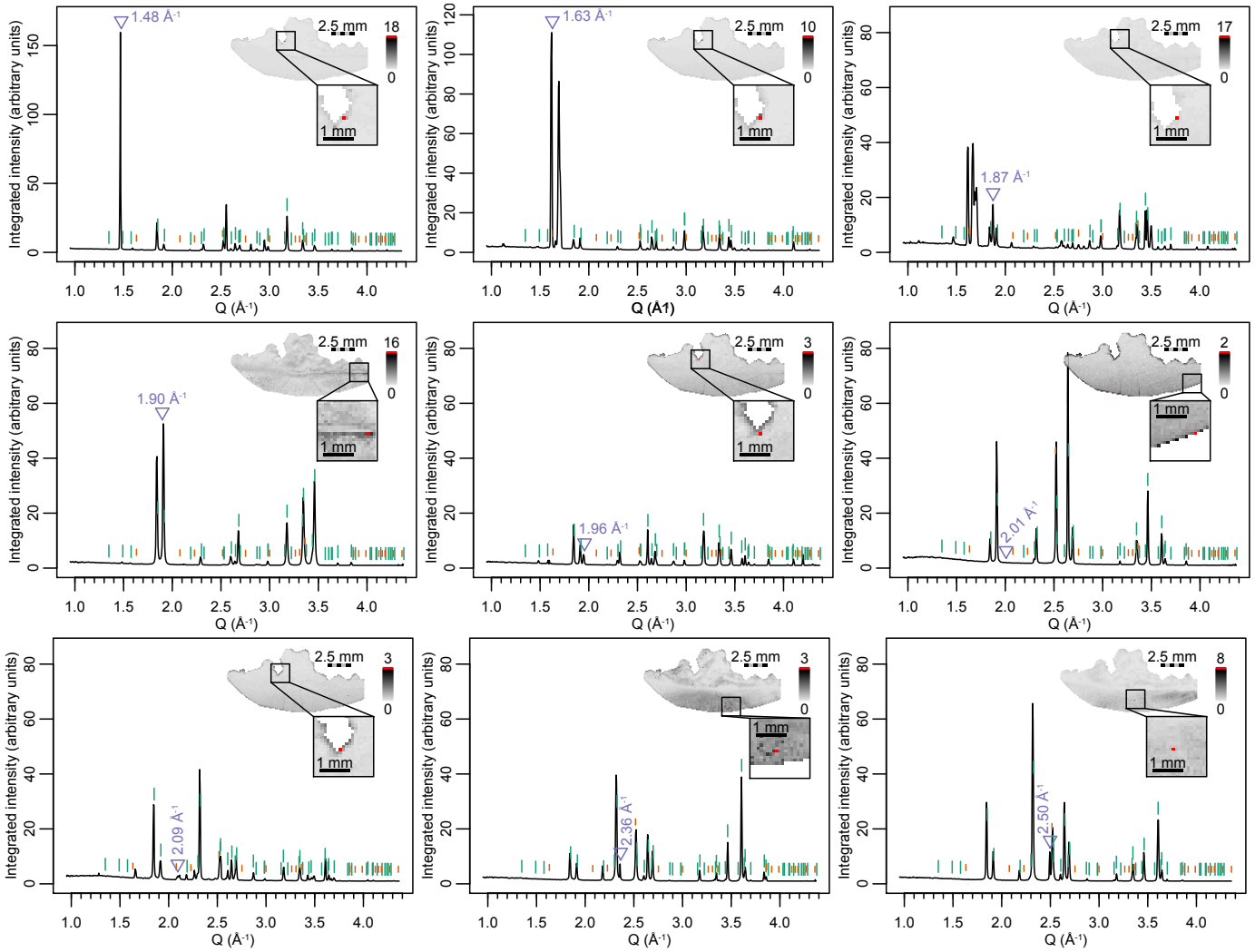

Figure S7
Identification and localisation of non-aragonite pixels in sample QCD.